materials

MDPI

Article

Microstructure and Mechanical Properties of $Co_{32}Cr_{28}Ni_{32.94}Al_{4.06}Ti_3$ High-Entropy Alloy

Jinquan Guo [1,2], Chaozhongzheng Tang [1] and Huan Sheng Lai [1,3,*]

[1] School of Mechanical Engineering and Automation, Fuzhou University, Fuzhou 350108, China; megjq@fzu.edu.cn (J.G.); n190227094@fzu.edu.cn (C.T.)
[2] Fujian Key Laboratory of Force Measurement, Fujian Metrology Institute, Fuzhou 350108, China
[3] Sino-French Institute of Nuclear Engineering and Technology, Sun Yat-sen University, Guangzhou 510275, China
* Correspondence: laihsh@mail.sysu.edu.cn

Abstract: High-entropy alloys have good application prospects in nuclear power plants due to their excellent mechanical properties and radiation resistance. In this paper, the microstructure of the $Co_{32}Cr_{28}Ni_{32.94}Al_{4.06}Ti_3$ high-entropy alloy was researched using metallurgical microscopy, X-ray diffraction, and scanning electron microscopy. The mechanical properties were tested using a Vickers microhardness tester and a tensile testing machine, respectively. The results showed that $Co_{32}Cr_{28}Ni_{32.94}Al_{4.06}Ti_3$ had a single-phase, disordered, face-centered, cubic solid-solution structure and was strengthened by solid solution. The alloy lattice parameter and density were estimated as 0.304 nm and 7.89 g/cm^3, respectively. The test results indicated that the alloy had satisfactory mechanical properties with yield stress and tensile strength of about 530 MPa and 985 MPa, respectively.

Keywords: microstructure; high-entropy alloy; mechanical property

Citation: Guo, J.; Tang, C.; Lai, H.S. Microstructure and Mechanical Properties of $Co_{32}Cr_{28}Ni_{32.94}Al_{4.06}Ti_3$ High-Entropy Alloy. *Materials* **2022**, *15*, 1444. https://doi.org/10.3390/ma15041444

Academic Editor: Jan Frenzel

Received: 22 December 2021
Accepted: 2 February 2022
Published: 15 February 2022

1. Introduction

High-entropy alloys (HEAs) are a type of alloys which contain five or more principle alloying elements to stabilize solid solution phases by maximizing configurational entropy. HEAs have been extensively studied since they were first reported in 2004 [1]. The novel design idea underlying HEAs has greatly expanded the composition range and research areas of metallic materials. Owing to the high entropy effect, the alloys tend to form simple microstructures, such as body-centered cubic (BCC), face-centered cubic (FCC), and densely packed hexagonal (HCP) [2,3]. It has been found that some HEAs not only have excellent mechanical properties [4,5], but also excellent thermal stability [5], wear resistance [4–7], and irradiation resistance. Therefore, HEAs are promising materials for application in nuclear power plants.

The phase composition and mechanical properties of HEAs are determined by the element types and their atomic ratios in the alloy [8]. For transition HEAs, $AlCoCrFeNiZr_x$ is known to possess a BCC structure when $x = 0$ [9]; with an increase in the Zr content, the mechanical properties are significantly improved, because the phase composition of the alloy changes from an ordered BCC solid-solution phase to an ordered Laves + BCC phase. The phase composition of the $AlCoCrFeNiB_x$ alloy changes from a BCC phase to BCC + FCC two-phase solid solution with an increase in the B content; meanwhile, the hardness and fracture strength increase first and then decrease [10]. $CoCrFeNiW_x$ is known to possess a single-phase structure for $x = 0.2$ [11]; the phase composition of the alloy changes from a single-phase to a hypoeutectic phase, and the mechanical properties are significantly improved when the W content is increased. The phase composition of $Al_xCoCrFeNiTi$ changes from α + Al grains to fine equiaxed crystals when the Al content is increased; in this way, the yield stress is increased, but the elongation is decreased [12].

AlFeCrCoNi only exhibits an FCC structure for a low ratio of Al/Ni. However, for a large ratio of Al/Ni, the alloy exhibits a BCC structure. The hardness increases with the increase in the ratio of Al/Ni [13].

The three-component alloy of CoCrNi has a single FCC structure. Its mechanical properties are better than other alloys in the alloy system, especially at liquid nitrogen temperature [14–16], but the strength is relatively low at chamber temperature [16]. The alloy used in this study is a new, unreported alloy with Al and Ti elements added. Therefore, in this paper, the microstructure and tensile properties of $Co_{32}Cr_{28}Ni_{32\cdot94}Al_{4\cdot06}Ti_3$ were researched in order to better understand the microstructure and mechanical properties of CoCrNi HEAs.

2. Experimental Materials and Methods

A $Co_{32}Cr_{28}Ni_{32\cdot94}Al_{4\cdot06}Ti_3$ plate with dimensions of 90 mm × 80 mm × 20 mm was prepared using vacuum arc melting equipment with pure metal Co, Cr, Ni, Al, and Ti with purities greater than 99.9 wt%. In order to ensure that the material was not oxidized in the melting process, pure metal Ti was melted firstly to absorb the residual gas of the electric arc furnace. The composition (atomic fraction and weight ratio, %) of the $Co_{32}Cr_{28}Ni_{32\cdot94}Al_{4\cdot06}Ti_3$ used in this study is shown in Table 1. The crystal structure was identified using a DY1602/Empyrean multifunctional X-ray polycrystalline diffractometer (PAnalytical, Alemlo, Holland) with Cu target radiation scanning in the range from 20° to 90° at a rate of 2°/min in a working voltage of 40 kV, a working current of 100 mA, and a characteristic wavelength of 1.5406 Å. The angle measurement accuracy was 0.02°. The HEA density was measured using a drainage method. In the drainage method, the mass of the HEA was measured by a scale; a measuring cylinder was used to measure the volume of water, and the volume of the HEA was the changed volume of the water in the cylinder before and after the HEA was put into the cylinder. The metallography of the HEA was characterized using a MV5000 metallographic microscope (Nanjing Lianchuang Analytical Instrument Manufacturing, Nanjing, China). The Vickers hardness of the HEA was measured using a THV-1MD microhardness tester (Teshi Detection Technology, Shanghai, China) under a load of 200 gf applied for 15 s. The tensile specimens with dimensions of 51.83 mm × 14 mm × 2.5 mm were used, as shown in Figure 1. Three tensile tests were carried out at air room temperature with a strain rate of 1×10^{-3} mm/s. The fracture morphology of the tensile specimen was analyzed using a Mira3 ultra-high-resolution field emission scanning electron microscope (FE-SEM) (TESCAN, Shanghai, China).

Table 1. Atomic and weight ratios of the principal elements of $Co_{32}Cr_{28}Ni_{32\cdot94}Al_{4\cdot06}Ti_3$.

Metal	Co	Cr	Ni	Al	Ti
Atomic ratio (%)	32	28	32.94	4.06	3
Weight ratio (%)	34.11	26.34	34.97	1.98	2.60

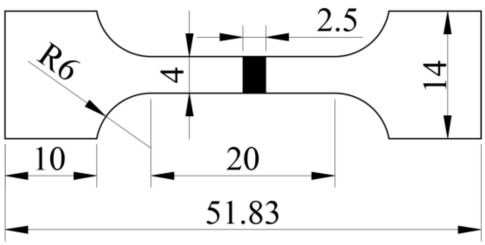

Figure 1. Dimensions of the tensile specimen (mm).

3. Results and Discussion

Figure 2 shows the X-ray diffraction (XRD) pattern of $Co_{32}Cr_{28}Ni_{32\cdot94}Al_{4\cdot06}Ti_3$, wherein three diffraction peaks corresponding to the (111), (200), and (220) peaks of the FCC struc-

ture were observed. There were no diffraction peaks corresponding to other structures. The result implies that the HEA was only composed of FCC solid solution.

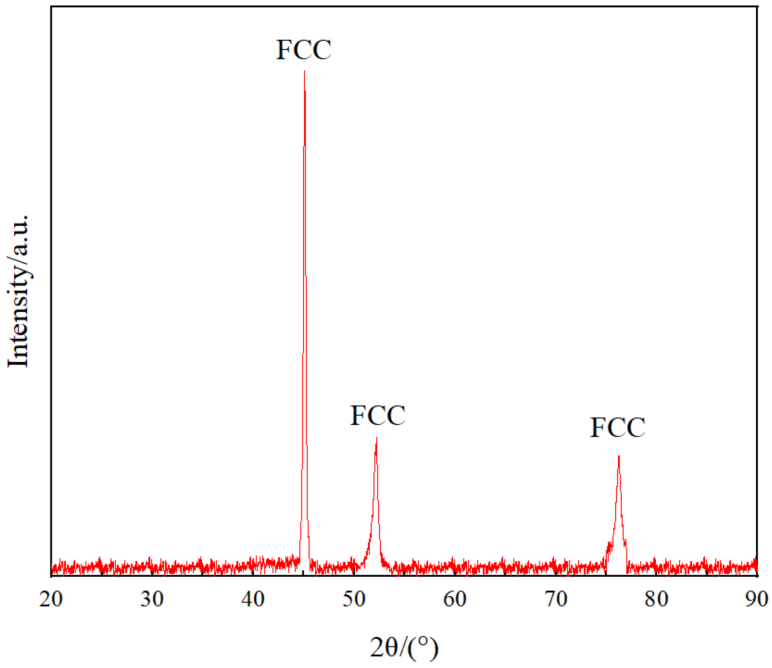

Figure 2. X-ray diffraction (XRD) results of $Co_{32}Cr_{28}Ni_{32\cdot94}Al_{4\cdot06}Ti_3$.

Generally, $\Omega > 1.1$ and $\delta < 6.5\%$ are the criteria for determining whether a solid solution phase can be formed [13]. Furthermore, when valence electron concentration (VEC) ≥ 8, the FCC solid solution is considered to be relatively stable [17]. The relevant parameters are calculated as follows:

$$\Delta H_{\text{mix}} = \sum_{i=1, i\neq j}^{n} \Delta H_{ij}^{\text{mix}} c_i c_j \quad (1)$$

$$\delta = \sqrt{\sum_{i=1}^{n} c_i \left(1 - r_i / \sum_{i=1}^{n} c_i r_i\right)^2} \quad (2)$$

$$\text{VEC} = \sum_{i=1}^{n} c_i (\text{VEC})_i \quad (3)$$

$$\Omega = \frac{T_m \Delta S_{\text{mix}}}{|\Delta H_{\text{mix}}|} \quad (4)$$

$$T_m = \sum_{i=1}^{n} c_i (T_m)_i \quad (5)$$

$$\Delta S_{\text{mix}} = -R \sum_{i=1}^{n} (c_i \ln c_i) \quad (6)$$

where ΔH_{mix} is the total enthalpy of mixing for the system, $\Delta H_{ij}^{\text{mix}}$ is the mixing enthalpy of the atomic pair of the ith and jth atoms, c_i and c_j are the atomic percentages of elements i and j, respectively, δ is the difference in atomic radius between the two atoms, r_i is the atomic radius of the ith element, VEC is the total VEC of the system, $(\text{VEC})_i$ is the VEC of the ith element, Ω is the disorder of the system, T_m is the mixed melting point of the system, ΔS_{mix} is the mixing entropy of the system, $(T_m)_i$ is the metal melting point of element i, and R is the gas constant.

Table 2 lists the characteristic parameters of the elements of $Co_{32}Cr_{28}Ni_{32\cdot94}Al_{4\cdot06}Ti_3$, and Table 3 lists the mixing enthalpy values of the atom pairs of the HEA elements [18].

According to the calculations, the difference in the atomic size (δ) of the HEA was 4.26%. The disorder of the system (Ω) of the HEA was 3.91, and the VEC of the HEA was 8.1. Therefore, the HEA considered here should be an FCC solid-solution structure in theory.

Table 2. Characteristic parameters of the principal elements of $Co_{32}Cr_{28}Ni_{32\cdot94}Al_{4\cdot06}Ti_3$.

Metal	Co	Cr	Ni	Al	Ti
Melting point (K)	1768.15	2132.15	1728.15	933.15	1941.15
Atomic radius [19,20] (nm)	0.125	0.128	0.123	0.143	0.147
VEC	9	6	10	3	4

Table 3. Mixed enthalpies among the principal elements of $Co_{32}Cr_{28}Ni_{32\cdot94}Al_{4\cdot06}Ti_3$ (kJ/mol).

Metal	Co	Cr	Ni	Al	Ti
Co	/	−4	0	−19	−28
Cr	−4	/	−7	−10	−7
Ni	0	−7	/	−22	−35
Al	−19	−10	−22	/	−30
Ti	−28	−7	−35	−30	/

The lattice constants of the five elements are listed in Table 4. The lattice constants of alloys can be calculated using the disorder principle [21]:

$$a_{\text{mix}} = \sum_{i=1}^{n} c_i a_i \tag{7}$$

where c_i is the atomic percentage of element i, and a_i is the lattice constants of element i. According to the calculations, the lattice constant of $Co_{32}Cr_{28}Ni_{32\cdot94}Al_{4\cdot06}Ti_3$ was 0.304 nm, which was consistent with the lattice constant obtained as per XRD analysis (Table 4).

Table 4. Densities and lattice constants of the component metals of $Co_{32}Cr_{28}Ni_{32\cdot94}Al_{4\cdot06}Ti_3$.

Metal	Co	Cr	Ni	Al	Ti	Alloy (Calculated)	Alloy (Measured)
Lattice constant (nm)	0.25	0.29	0.35	0.41	0.35	0.30	0.31
Density (g/cm^3)	8.90	7.19	8.90	2.70	4.54	7.85	7.84

The theoretical density of the alloy was calculated using the following formula [22]:

$$\rho_{\text{mix}} = \frac{\sum_{i=1}^{n} c_i A_i}{\sum_{i=1}^{n} c_i A_i / \rho_i} \tag{8}$$

where c_i is the atomic percentage of element i, A_i is the atomic weight of element i, and ρ_i is the density of element i. From the calculation results, we noted that the theoretical density (7.85 g/cm^3) of the HEA was almost identical to the measured value (7.84 g/cm^3). It was also found that the HEA results were consistent with the rule of mixtures upon comparing the lattice constant and theoretical density of the alloy, which was a disordered FCC solid-solution structure.

Figure 3 shows a light microscopy image of the metallographic structure of $Co_{32}Cr_{28}Ni_{32\cdot94}Al_{4\cdot06}Ti_3$. As shown in Figure 3, the alloy had a uniform, single-phase, equiaxial crystal structure, and the grain size was about 163 μm as measured using the transection method.

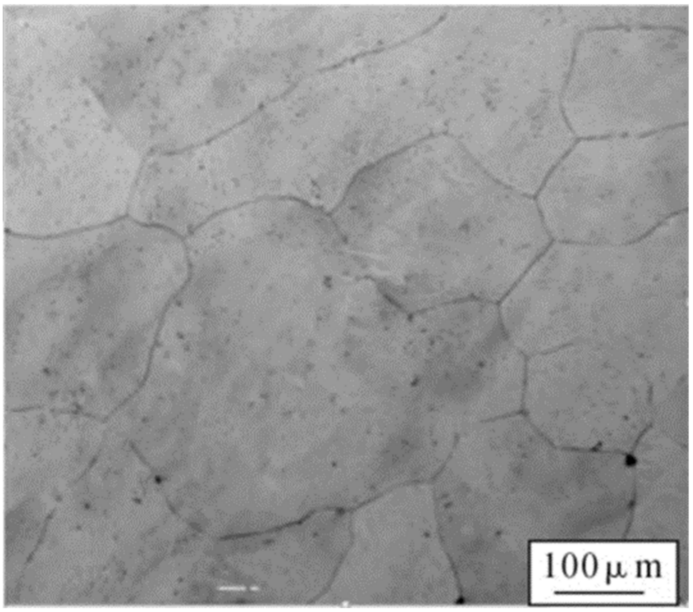

Figure 3. Microstructure of $Co_{32}Cr_{28}Ni_{32.94}Al_{4.06}Ti_3$.

Figure 4 shows the tensile stress–strain curve of $Co_{32}Cr_{28}Ni_{32.94}Al_{4.06}Ti_3$. As shown in Figure 4, the yield strength was 530 ± 6 MPa, the tensile strength was 985 ± 7 MPa, and the elongation was 37.16 ± 0.17%. Compared with the CoCrNi alloy, the yield strength and the tensile strength increased by 103% and 14%, while the elongation decreased by 7%. Obviously, the increase in Al and Ti elements improved the tensile properties of the CoCrNi baselime alloy. Moreover, from Table 5, which compares the uniaxial tensile test results of similar alloys, it can be seen that the alloy affords better strength and plasticity. Moreover, the microhardness of the alloy was 313 HV. Therefore, $Co_{32}Cr_{28}Ni_{32.94}Al_{4.06}Ti_3$ exhibits satisfactory tensile mechanical properties and hardness.

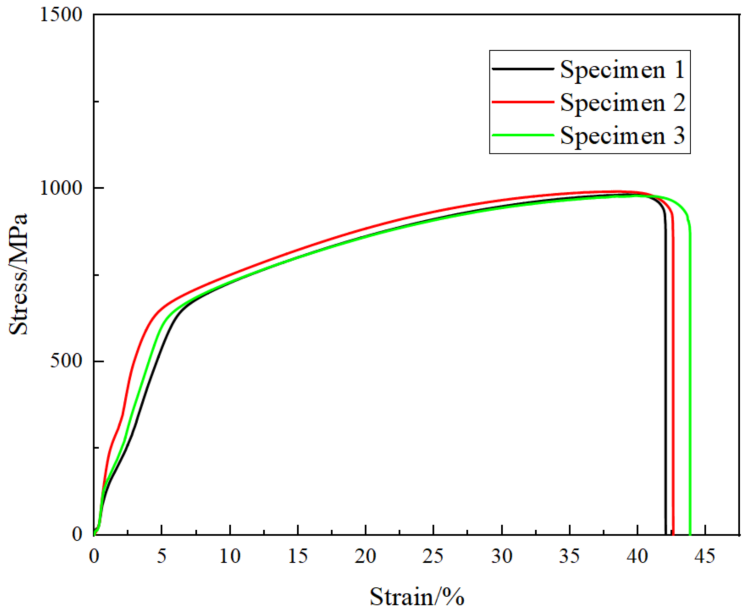

Figure 4. Stress–strain curve of $Co_{32}Cr_{28}Ni_{32.94}Al_{4.06}Ti_3$.

Table 5. Comparison of the tensile mechanical properties.

Alloy	Yield Strength (MPa)	Tensile Strength (MPa)	Elongation to Failure (%)
$Co_{32}Cr_{28}Ni_{32.94}Al_{4.06}Ti_3$	530 ± 6	985 ± 7	37.2 ± 0.17
CoCrNi [15]	260	870	40
$(Fe_{50}Mn_{30}Co_{10}Cr_{10})_{94}C_6$ [23]	450	700	18
$CoCrFeNiW_{0.4}$ [10]	525	970	11
$Al_3CoCrFeNiTi$ [11]	115	152	26
CoCrFeMnNi [24]	468	590	30
N18 Zircaloy [25]	390	420	38
N36 Zircaloy [25]	310	520	27

The tensile properties of the $Co_{32}Cr_{28}Ni_{32.94}Al_{4.06}Ti_3$ studied in this paper are obviously improved compared with N18 and N36 Zircaloy currently used in the nuclear industry, as shown in Table 5. Therefore, the alloy studied in this paper is could be used in the nuclear industry.

Generally, the main strengthening mechanism of a single disordered FCC solid-solution structure is solid-solution strengthening, which mainly originates from the interaction between solute atoms [26].

Figure 5 shows an SEM micrograph of the fractured tensile specimen of $Co_{32}Cr_{28}Ni_{32.94}Al_{4.06}Ti_3$. A large number of dimples and holes were observed in the fracture. The observed dimples were the traces left on the fracture after micropore nucleation and aggregation, which was the characteristic of micropore aggregation fractures.

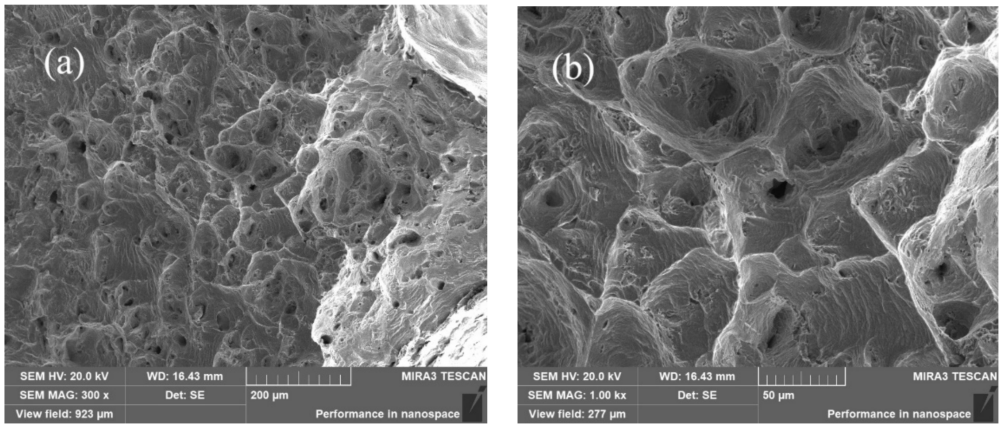

Figure 5. Scanning electron microscopy (SEM) images of the fracture surface of $Co_{32}Cr_{28}Ni_{32.94}Al_{4.06}Ti_3$. (**a**) magnification of 300 times; (**b**) magnification of 1000 times.

The results provide a reference for the study of microstructure and properties of CoCrNi HEAs. In order to fully explain the comprehensive mechanical properties of the HEA, further studies on CoCrNiAlTi HEAs are being carried out, such as the effects of different atomic ratios of major elements on the creep, fatigue properties, and irradiation resistance of CoCrNiAlTi HEAs.

4. Conclusions

In this paper, the microstructure and tensile-fracture characteristics of $Co_{32}Cr_{28}Ni_{32.94}Al_{4.06}Ti_3$ were researched. The following conclusions can be drawn:

(1) The $Co_{32}Cr_{28}Ni_{32.94}Al_{4.06}Ti_3$ exhibits a single disordered FCC solid-solution structure with a density of 7.89 g/cm^3.

(2) The microstructure of $Co_{32}Cr_{28}Ni_{32.94}Al_{4.06}Ti_3$ is equiaxed, with a grain size about 163 µm.

(3) The yield strength, tensile strength, and elongation of the $Co_{32}Cr_{28}Ni_{32.94}Al_{4.06}Ti_3$ are about 530 MPa, 985 Mpa, and 37.2%, respectively. The microhardness of the alloy is 313 HV.

Author Contributions: Conceptualization, J.G. and H.S.L.; methodology, J.G. and C.T.; experiment, C.T.; writing—original draft preparation, C.T.; writing—review and editing, J.G. and H.S.L. All authors listed have made a substantial, direct, and intellectual contribution to the work. All authors have read and agreed to the published version of the manuscript.

Funding: The authors are grateful to the National Natural Science Foundation of China (No. 11972005 and No. 51675103), the 2021 Independent Innovation Fund of Tianjin University-Fuzhou University (Grant Number TF2021-5), and the Open Fund of Fujian Key Laboratory of Force Measurement (Fujian Metrology Institute) (FJLZSYS202102) for the financial support to this study.

Institutional Review Board Statement: Not applicable.

Informed Consent Statement: Not applicable.

Data Availability Statement: Not applicable.

Conflicts of Interest: No potential conflict of interest was reported by the authors.

References

1. Yeh, J.W.; Chen, S.K.; Lin, S.J.; Gan, J.Y.; Chin, T.S.; Shun, T.T.; Tsau, C.H.; Chang, S.Y. Nanostructured high-entropy alloys with multiple principal elements: Novel alloy design concepts and outcomes. *Adv. Eng. Mater.* **2004**, *6*, 299–303. [CrossRef]
2. Schuh, B.; Mendez-Martin, F.; Völker, B.; George, E.P.; Clemens, H.; Pippan, R.; Hohenwarter, A. Mechanical properties, microstructure and thermal stability of a nanocrystalline CoCrFeMnNi high-entropy alloy after severe plastic deformation. *Acta Mater.* **2015**, *96*, 258–268. [CrossRef]
3. Lu, Y.P.; Gao, X.Z.; Jiang, L.; Zhen, Z.; Tang, T.; Jie, J.; Kang, H.; Zhang, Y.; Guo, S.; Ruan, H. Directly cast bulk eutectic and near-eutectic high entropy alloys with balanced strength and ductility in a wide temperature range. *Acta Mater.* **2017**, *124*, 143–150. [CrossRef]
4. Chou, Y.L.; Wang, Y.C.; Yeh, J.W.; Shih, H.C. Pitting corrosion of the high-entropy alloy $Co_{1.5}CrFeNi_{1.5}Ti_{0.5}Mo_{0.1}$ in chloride-containing sulphate solutions. *Corros. Sci.* **2010**, *52*, 3481–3491. [CrossRef]
5. Varalakshmi, S.; Kamaraj, M.; Murty, B.S. Processing and properties of nanocrystalline CuNiCoZnAlTi high entropy alloys by mechanical alloying. *Mater. Sci. Eng. A* **2010**, *527*, 1027–1030. [CrossRef]
6. Senkov, O.N.; Woodward, C.F. Microstructure and properties of a refractory $NbCrMo_{0.5}Ta_{0.5}TiZr$ alloy. *Mater. Sci. Eng. A* **2011**, *529*, 311–320. [CrossRef]
7. Varalakshmi, S.; Appa Rao, G.; Kamaraj, M.; Murty, B.S. Hot consolidation and mechanical properties of nanocrystalline equiatomic AlFeTiCrZnCu high entropy alloy after mechanical alloying. *J. Mater. Sci.* **2010**, *45*, 5158–5163. [CrossRef]
8. Guo, S.; Liu, C.T. Phase stability in high entropy alloys: Formation of solid-solution phase or amorphous phase. *Prog. Nat. Sci. Mater.* **2011**, *21*, 433–446. [CrossRef]
9. Chen, J.; Niu, P.Y.; Liu, Y.Z.; Lu, Y.K.; Wang, X.H.; Peng, Y.L.; Liu, J.N. Effect of Zr content on microstructure and mechanical properties of AlCoCrFeNi high entropy alloy. *Mater. Design* **2016**, *94*, 39–44. [CrossRef]
10. Chen, Q.S.; Lu, Y.P.; Dong, Y.; Wang, T.M.; Li, T.J. Effect of minor B addition on microstructure and properties of AlCoCrFeNi multi-compenent alloy. *Trans. Nonferr. Met. Soc.* **2015**, *25*, 2958–2964. [CrossRef]
11. Wang, L.; Wang, L.; Tang, Y.C.; Luo, L.; Luo, L.S.; Su, Y.Q.; Guo, J.J.; Fu, H.Z. Microstructure and mechanical properties of $CoCrFeNiW_x$ high entropy alloys reinforced by μ phase particles. *J. Alloys Compd.* **2020**, *845*, 155997. [CrossRef]
12. Li, Q.L.; Zhao, S.; Bao, X.P.; Zhang, Y.S.; Zhu, Y.Q.; Wang, C.Z.; Lan, Y.F.; Zhang, Y.X.; Xia, T.D. Effects of AlCoCrFeNiTi high-entropy alloy on microstructure and mechanical properties of pure aluminum. *J. Mater. Sci. Technol.* **2020**, *52*, 1–11. [CrossRef]
13. Harihar, S.; Joseph, W.N.; Frank, L.F. Microstructural characterization and mechanical properties of laser deposited high entropy alloys. *Mater. Sci. Forum.* **2014**, *3129*, 2370–2375.
14. Gludovatz, B.; Hohenwarter, A.; Thurston KV, S.; Bei, H.B.; Wu, Z.G.; George, E.P.; Ritchie, R.O. Exceptional damage-tolerance of a medium-entropy alloy CrCoNi at cryogenic temperatures. *Nat. Commun.* **2016**, *7*, 10602. [CrossRef]
15. Wu, Z.; Bei, H.; Pharr, G.M.; George, E.P. Temperature dependence of the mechanical properties of equiatomic solid solution alloys with face-centered cubic crystal structures. *Acta Mater.* **2014**, *81*, 428–441. [CrossRef]
16. Wu, Z.; Bei, H.; Otto, F.; Pharr, G.M.; George, E.P. Recovery, recrystallization, grain growth and phase stability of a family of FCC-structured multi-component equiatomic solid solution alloys. *Intermetallics* **2014**, *46*, 131–140. [CrossRef]
17. Guo, S.; Ng, C.; Lu, J.; Liu, C.T. Effect of valence electron concentration on stability of bcc or fcc phase in high entropy alloys. *J. Appl. Phys.* **2011**, *109*, 103505. [CrossRef]
18. Takeuchi, A.; Inoue, A. Classification of bulk metallic glasses by atomic size difference, heat of mixing and period of constituent elements and its application to characterization of the main alloying element. *Mater. Trans.* **2005**, *46*, 2817–2829. [CrossRef]
19. Pauling, L. Atomic Radii and Interatomic Distances in Metal. *J. Am. Chem. Soc.* **1947**, *69*, 542–553. [CrossRef]

20. Petrucci, R.H.; Harwood, W.S.; Geoffery, F.H.; Jeffry, D. Madura. In *General Chemistry*, 9th ed.; Pearsin Prentice Hall: Hoboken, NJ, USA, 2007.
21. Juan, C.C.; Tsai, M.H.; Tsai, C.W.; Lin, C.M.; Wang, W.R.; Yang, C.C.; Chen, S.K.; Liu, S.J.; Yeh, J.W. Enhanced mechanical properties of HfMoTaTiZr and HfMoNbTaTiZr refractory high-entropy alloys. *Intermetallics* **2015**, *62*, 76–83. [CrossRef]
22. Huang, H.; Wu, Y.; He, J.; Wang, H.; Liu, X.; An, K.; Wu, W.; Lu, Z. Phase-transformation ductilization of brittle high-entropy alloys via metastability engineering. *Adv. Mater.* **2017**, *29*, 1701678. [CrossRef] [PubMed]
23. Liu, X.L.; Zhao, X.R.; Chen, J.; Lv, Y.K.; Wang, X.H.; Liu, B.; Liu, Y. Effect of C addition on microstructure and mechanical properties of as-cast HEAs $(Fe_{50}Mn_{30}Co_{10}Cr_{10})_{100-x}C_x$. *Mater. Chem. Phys.* **2020**, *254*, 123501. [CrossRef]
24. Listyawan, T.A.; Lee, H.; Park, N.; Lee, U. Microstructure and mechanical properties of CoCrFeMnNi high entropy alloy with ultrasonic nanocrystal surface modification process. *J. Mater. Sci. Technol.* **2020**, *57*, 123–130. [CrossRef]
25. Nikulina, A.V. Zirconium alloy in nuclear power engineering. *Met. Sci. Heat Treat.* **2004**, *46*, 458–462. [CrossRef]
26. Tian, F.Y.; Varga, L.K.; Chen, N.X.; Shen, J.; Vitos, L. Empirical design of single phase high-entropy alloys with high hardness. *Intermetallics* **2015**, *58*, 1–6. [CrossRef]